International Journal of Fluid Power 8 (2007) No. 2 pp. 37-46

EXPERIMENTS AND CFD SIMULATIONS FOR THE CHARACTERISATION OF THE ORIFICE FLOW IN A FOUR-WAY SERVOVALVE

Gianpietro Di Rito

Department of Aerospace Engineering – University of Pisa, via Caruso, 56122 Pisa, Italy
g.dirito@ing.unipi.it

Abstract

It is well-known that the discharge efficiency of an orifice varies with the flow condition: it is very low for laminar flow, it reaches a maximum in "mixed" conditions, and it tends to be constant (i.e. insensitive to flow variations) when turbulence is fully developed. However, the classical approach to the modelling of servo-hydraulic actuators is based on the hypothesis that the flow through the servovalve orifices is turbulent, and this assumption can lead to significant errors if the dynamics of actuators operating in extreme conditions is concerned. This is the case of aerospace applications, since flight actuators can be commanded to move against high counteracting loads or at very low velocities, and a laminar (or rather "mixed") flow pattern can be established in the servovalve orifices. In the paper, the flow through the Moog D633 four-way servovalve is studied by means of experiments and Computational Fluid Dynamics simulations (developed in the STAR-CD environment). Two are the basic objectives of the investigation: to characterise the laminar-to-turbulent flow transition in the orifices of an aircraft-type hydraulic component, providing an original physical interpretation to the increase of the orifice discharge efficiency in "mixed" flow conditions, and to highlight the necessity of using Reynolds-dependant orifice equations for the modelling of high-performance servo-hydraulic actuators.

Keywords: orifice flow, CFD analysis, experiments on hydraulic fluids, laminar-to-turbulent transition, electro-hydraulic servovalve

1 Introduction

The well-known relationship between the flow rate and the pressure drop through an orifice is described by Eq. 1 and 2,

$$Q_o = K_o \sqrt{\Delta P_o} \tag{1}$$

$$K_o = C_{do} \sqrt{2/\rho} A_o \tag{2}$$

where Q_o, ΔP_o and K_o respectively represent the flow rate, the pressure drop and the leakage coefficient of the orifice, ρ is the fluid density, A_o is the orifice area, and C_{do} is the orifice discharge coefficient. The discharge coefficient provides an estimate of the energy dissipation related to the orifice flow, so that the higher is C_{do} the lower is the dissipation (i.e. the heat generation).

Experiments and theoretical studies indicate that the discharge coefficient basically depends on the orifice geometry (shape of the conduits, shape of the walls, orifice edges, etc.), and on the Reynolds number. In particular, the discharge coefficient is very low for laminar flow, it typically reaches a maximum in "mixed" conditions, and it tends to be constant (i.e. insensitive to flow variations) when turbulence is fully developed.

However, the Reynolds-dependence of the discharge coefficient is usually disregarded in hydraulic systems modelling, since for the most applications the flow through an orifice is turbulent, and the discharge coefficient can be assumed to be constant. This approach is used also for the modelling of servo-hydraulic actuators, so that the flow through the servovalve orifices is modelled by assuming that the flow rates only depend on the orifice area and on the square root of the pressure drop. This assumption is applicable in many practical cases, but it is erroneous if the dynamics of actuators operating in extreme conditions is concerned. In aerospace applications, flight actuators can be commanded to move the aerodynamic control surfaces against high counteracting loads or at very low velocities, so that a laminar (or rather "mixed") flow pattern can be established in the servovalve orifices. A laminar transition of the orifice flow implies a variation of the discharge characteristics, which generally induces a variation of the actuator position response.

Apart from classical literature references (Merritt, 1967), other authors recently studied the flow through

This manuscript was received on 20 February 2007 and was accepted after revision for publication on 12 June 2007

servovalves, focusing the attention on the experimental determination of the orifice discharge coefficients (Viall and Zhang, 2000), on the evaluation of the flow forces acting on the servovalve spool via numerical simulations (Baudry and Mare, 2000; Del Vescovo, 2004) or on the development of empirical Reynolds-dependant orifice equations for servovalve modelling (Borutzky et al., 2002). Nevertheless, information about the physical interpretation of the phenomena characterising the laminar-to-turbulent transition (e.g. the increase of the discharge efficiency in "mixed" flow conditions) are scarce.

In the paper, the flow through the Moog D633 four-way servovalve is studied by means of experiments and Computational Fluid Dynamics (CFD) simulations. Two are the basic objectives of the investigation: to characterise the laminar-to-turbulent transition in the orifices of an aircraft-type hydraulic component, providing an original physical interpretation to the increase of the discharge efficiency in "mixed" flow conditions, and to highlight the necessity of using Reynolds-dependant orifice equations for the modelling of high-performance servo-hydraulic actuators.

2 Experimental Characterisation

2.1 Experimental Set-up

Figure 1 shows the experimental set-up used for the characterisation of the flow through the Moog D633 servovalve.

The test bench is equipped with four pressure transducers (one for each of the four ways of the servovalve), two flow transducers (the one mounted between the load ports, the other on the return), and two temperature gauges (the one mounted on the supply, the other on the return). Furthermore, a pressure-compensated flow regulating valve is mounted between the load ports, in order to perform the tests with a fixed value of the load flow rate, despite the value of the pressure drop that is applied on the valve itself. The bench is supplied with MIL-H-5606B fluid by a variable displacement pump, which is capable to provide flow rates up to 100 l/min at a fluid pressure of 210 bar.

The test campaign is performed by collecting the spool positions (measured by the integrated LVDT transducer of the servovalve), the flow rates, the pressures and the temperatures as static measurements in different sessions. For each session, the opening of the flow regulating valve is fixed and the servovalve spool is stepwise driven from the centred to the fully-opened condition. Once the spool is driven back to the null position, the opening of the flow regulating valve is changed and another session of measurements is started.

2.2 Estimation of the Leakage Coefficients

As discussed in section 1, the flow through the *i*-th servovalve orifice can be described by Eq. 3, so the servovalve flow is fully characterised if the four leakage coefficients K_i are known.

$$Q_i = K_i \sqrt{\Delta P_i} \quad \forall \; i = 1 \,,\ldots,\; 4 \tag{3}$$

The problem is that no direct measurement of the local flow rates Q_i is available with the test bench shown in Fig. 1, so some simplifying assumptions must be introduced in order to estimate the leakage coefficients.

With reference to the simplified scheme of the servovalve flow shown in Fig. 2, Eq. 4 and 5 represents the mass conservation equations in the case of direct connection between the load ports (the test bench case).

$$Q_A = Q_1 - Q_4 = Q_3 - Q_2 = Q_B \tag{4}$$

$$Q_R = Q_{RA} + Q_{RB} = Q_3 + Q_4 \tag{5}$$

Assuming that the spool displacement (x_v) induces a symmetrical valve opening (i. e. $A_1(x_v) = A_2(-x_v) = A_3(x_v) = A_4(-x_v)$) and considering that the leakage coefficients basically depend on the orifice areas (Eq. 2), Eq. 4 and 5 can be re-written in the form given by Eq. 6 and 7,

$$Q_A = K_1 \sqrt{P_S - P_A} - K_2 \sqrt{P_A - P_R} \tag{6}$$

$$Q_R = K_1 \sqrt{P_B - P_R} + K_2 \sqrt{P_A - P_R} \tag{7}$$

which provide a simplified model of the servovalve flow, characterised by only two leakage coefficients.

For a correct estimation of the leakage coefficients, the four pressures appearing in Eq. 6 and 7 should be referred to the valve ports, while on the test bench the pressures are measured at a certain distance from them, Fig. 1. For this reason, the actual valve pressures (P) have been estimated by adding (or subtracting) to the measurements ($P^{(m)}$) the pressure drops due to the pipeline between the valve ports and the related transducers, Eq. 8 and 11.

$$P_S = P_S^{(m)} - \frac{8\ \rho\ L_S\ \lambda_S\ Q_R^{\,2}}{\pi^2\ D_S^{\,5}} \tag{8}$$

$$P_A = P_A^{(m)} + \frac{8\ \rho\ L_L\ \lambda_L\ Q_A^{\,2}}{\pi^2\ D_L^{\,5}} \tag{9}$$

$$P_B = P_B^{(m)} - \frac{8\ \rho\ L_L\ \lambda_L\ Q_A^{\,2}}{\pi^2\ D_L^{\,5}} \tag{10}$$

$$P_R = P_R^{(m)} + \frac{8\ \rho\ L_R\ \lambda_R\ Q_R^{\,2}}{\pi^2\ D_R^{\,5}} \tag{11}$$

In Eq. 8 and 11, L represent the pipes' lengths, D are the pipes' diameters (see the data reported in Fig. 1), and λ are the pressure loss coefficients, which have been estimated by Eq. 12 (a linear interpolation between the values $\lambda(2000)$ and $\lambda(4000)$ has been used when Re lied in the uncertainty range) as functions of the pipes' Reynolds numbers, Eq. 13.

$$\lambda = \begin{cases} \dfrac{64}{Re} & Re \le 2000 \\ \\ \dfrac{0.3164}{Re^{0.25}} & Re \ge 4000 \end{cases} \tag{12}$$

$$Re = \frac{4\ Q}{\pi\ D\ \nu} \tag{13}$$

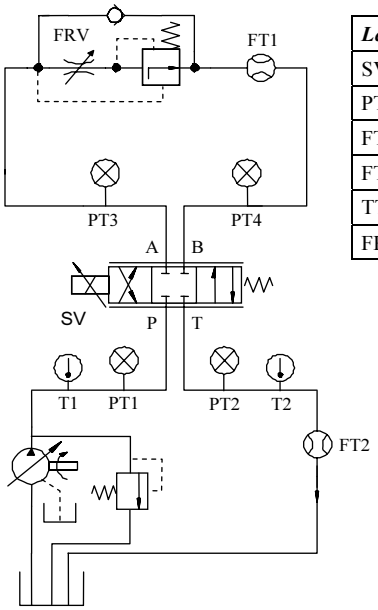

Legend
SV: MOOG D633-313-B Servovalve (Nominal flow rate: 40 l/min @ ΔP=35 bar)
PT1-PT4: Pressure transducers Keller PA-23-S (Max pressure 250 bar)
FT1: Flow Transducer VSE VS02-GP012 (Max flow rate 18 l/min)
FT2: Flow Transducer Kracht VC1-F1-P5-A01 (Max flow rate 50 l/min)
TT1-TT2: Temperature Transducers
FRV: Flow Regulating Valve Rexroth 2FRM-6-B763X/25QRV (Range: 0÷25 l/min)

Pipe	*Diameter*	*Length*
PT1 – P	6.4 mm	85 mm
PT2 – T	9.5 mm	85 mm
PT3 – A	8 mm	85 mm
PT4 – B	8 mm	85 mm

(a) Hydraulic scheme

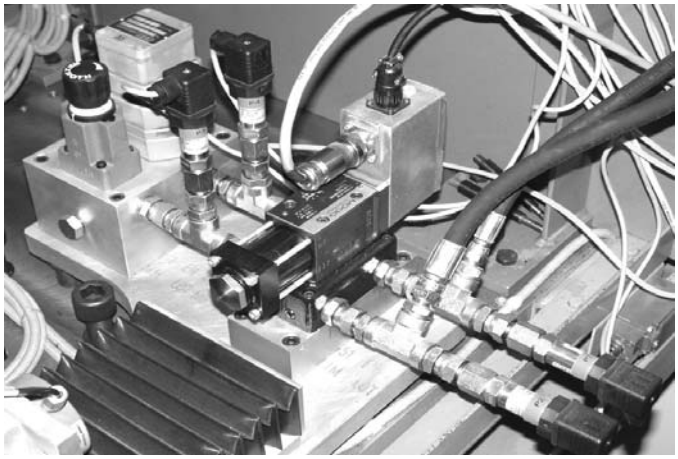

(b) Overall view

Fig. 1: *Test bench for the experimental characterisation of the servovalve flow*

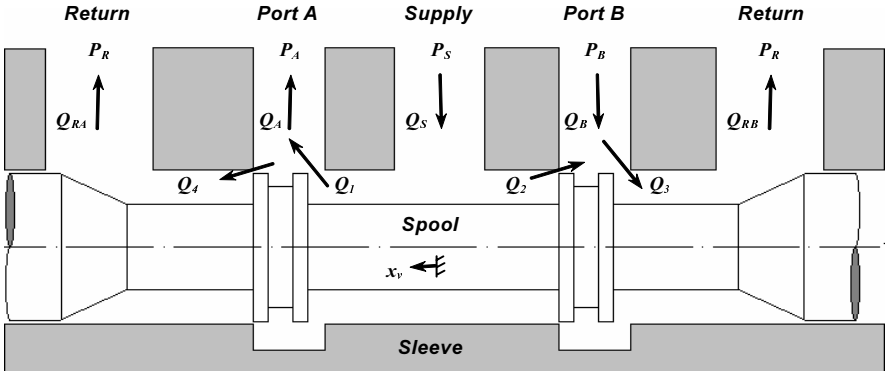

Fig. 2: *Simplified scheme of the servovalve flow*

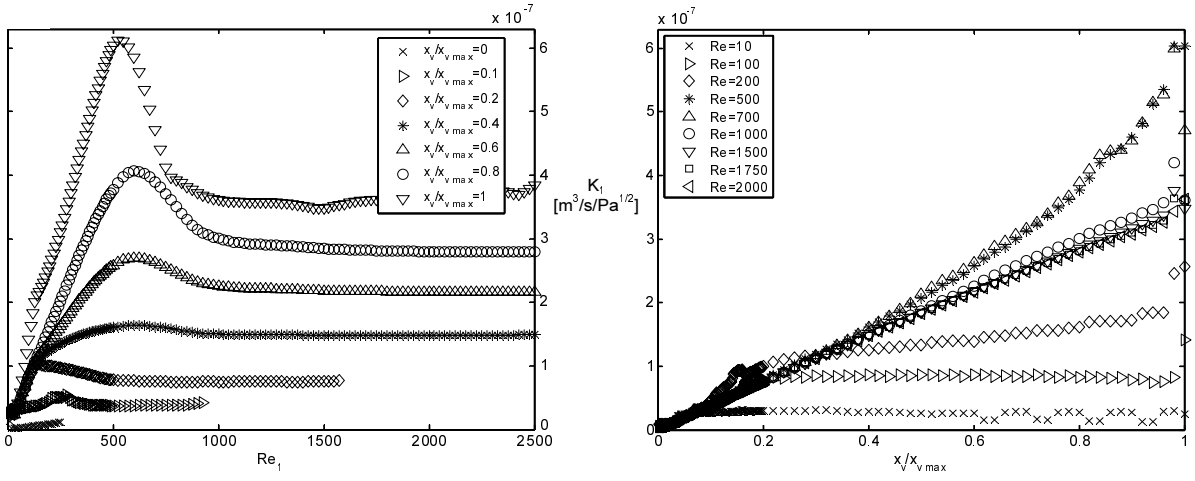

(a) (b)

Fig. 3: *Experimental results: relation between leakage coefficient, spool position and Reynolds number for orifice 1 (supply-port A and port B-return)*

In Eq. 13, the fluid kinematic viscosity (v) has been evaluated by assuming a reference density and by estimating the absolute viscosity from the mean value of the temperature measurements obtained on the bench.

Once obtained the leakage coefficients from Eq. 6 and 13, the related discharge coefficients have been calculated by Eq. 2, considering that the orifice areas were given by the measured spool position. Finally, in order to obtain an experimental evidence of the dependence of the leakage coefficients on the flow condition, the orifice Reynolds numbers have been evaluated by Eq. 14 and 15, where w is the area gradient of the valve orifices.

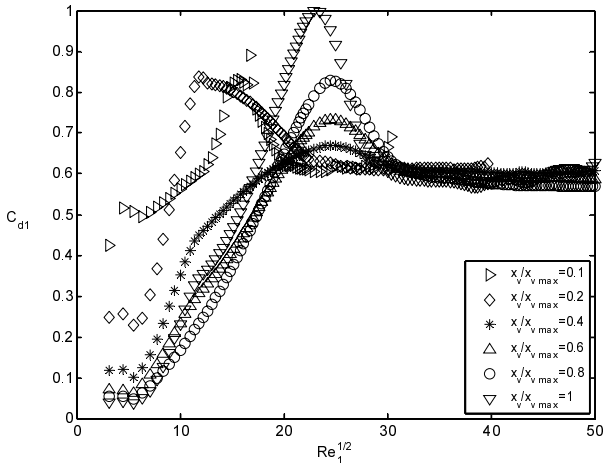

Fig. 4: *Experimental results: discharge coefficient as a function of Reynolds number for orifice 1 (supply-port A and port B-return)*

$$Re_1 = \frac{2\ |Q_1|}{\nu\ (w + x_v)} \cong \frac{|Q_R + Q_A|}{\nu\ (w + x_v)} \tag{14}$$

$$Re_2 = \frac{2\ |Q_2|}{\nu\ (w + x_v)} \cong \frac{|Q_R - Q_A|}{\nu\ (w + x_v)} \tag{15}$$

2.3 Experimental Results

Figure 3.a reports the leakage coefficient related to orifice 1 (supply-port A and port B-return) plotted as a function of the orifice Reynolds number for different spool positions, while Fig. 3.b shows the same quantity as a function of the spool position for different Reynolds numbers (The repeatability of the experimental data is of about 1 %).

Experiments point out that the servovalve flow can be considered turbulent only for Re > 1000: actually, the leakage coefficient is both constant with Reynolds numbers and roughly linear with the spool position (i. e. with the orifice area). On the other hand, if lower flow rates are concerned, the leakage coefficient exhibits a significant dependence from Reynolds number, and a laminar-to-turbulent transition occurs.

This phenomenon is highlighted by the plot reported in Fig. 4, where the discharge coefficient C_{d1} is plotted as a function of the square root of the orifice Reynolds number Re_1. The plot is rather popular in hydraulics, since the discharge coefficient linearly depends on the square root of the Reynolds number if the flow is totally laminar, while it is constant if the flow is completely turbulent (Merritt 1967). Figure 4 clearly shows that the servovalve flow is characterised by laminar (see the range of $Re_1 < 200$) as well as turbulent (see the range of $Re_1 > 1000$) conditions, and the transition between these phases includes an increase of the discharge efficiency at intermediate Reynolds numbers.

3 CFD Simulation

The numerical simulation of the servovalve flow has been obtained by means of the STAR-CD software (version 3.150), starting from a CAD model of the spool-sleeve assembly, developed in the CATIA environment. STAR-CD has been used for both the generation of the mesh and the flow simulation, by using the PROSTAR toolbox and the PRO-AM toolbox respectively.

3.1 CFD Model

Figure 5 shows general and detailed views of the spool and the sleeve of the servovalve. The components are characterised by extremely small clearances (the radial gap and the orifice underlap are in the range of some microns), so their dimensions have been determined using a high-precision contact-measurement machine, which provides an accuracy of about 0.5 microns.

Considering that the components are 90°-rotational symmetric and assuming the spool position as a variable parameter of the analysis, different CATIA models reproducing one-quarter of the actual valve assembly have been developed and imported in the STAR-CD environment.

The tetrahedrical-shaped volume mesh has been automatically generated by the PROSTAR toolbox, starting from a user-defined surface mesh, in which a special refinement has been imposed in the vicinity of the valve orifices, Fig. 6.

It is to be mentioned that, before creating the surface mesh, the model has been scaled up by ten times, in order to overcome a software limitation on the maximum flattening level of the model elements, which would have generally implied a limitation on the mesh refinement level.

Since the number of elements of the models varied from about 550 thousands (for the model representing a centred valve spool) to about 1 billion (for the model with a fully-opened valve), high computing resources have been necessary for the CFD simulations. As an example, a PC equipped with a 2.66 GHz Intel XEON CPU and a 4 GB RAM took about 30 hours to run one simulation.

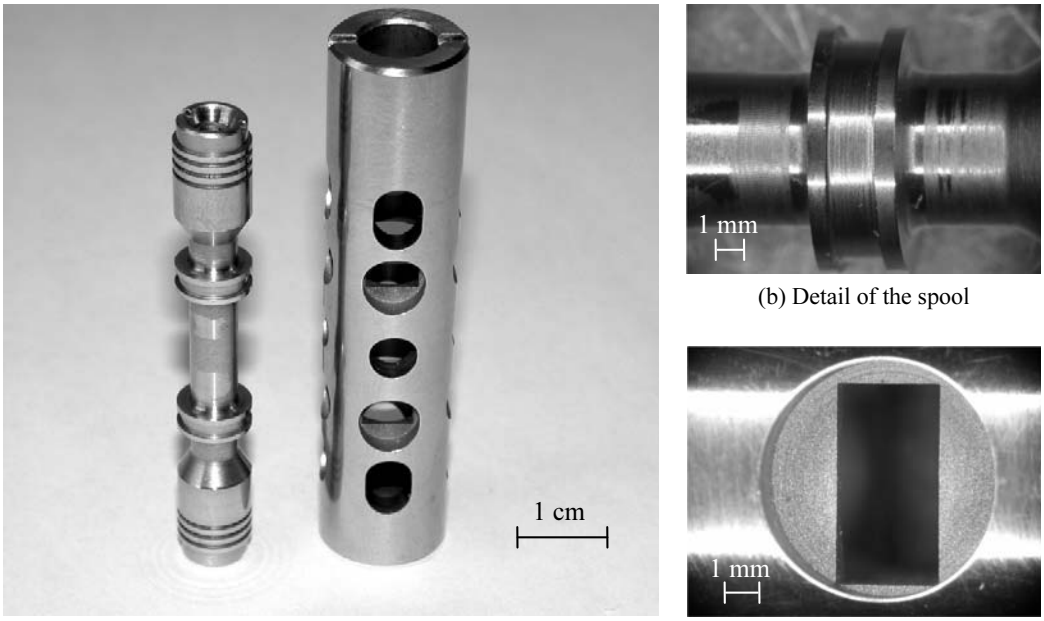

(a) General view (b) Detail of the spool (c) Detail of the sleeve

Fig. 5: *Spool and sleeve of the Moog D633 servovalve*

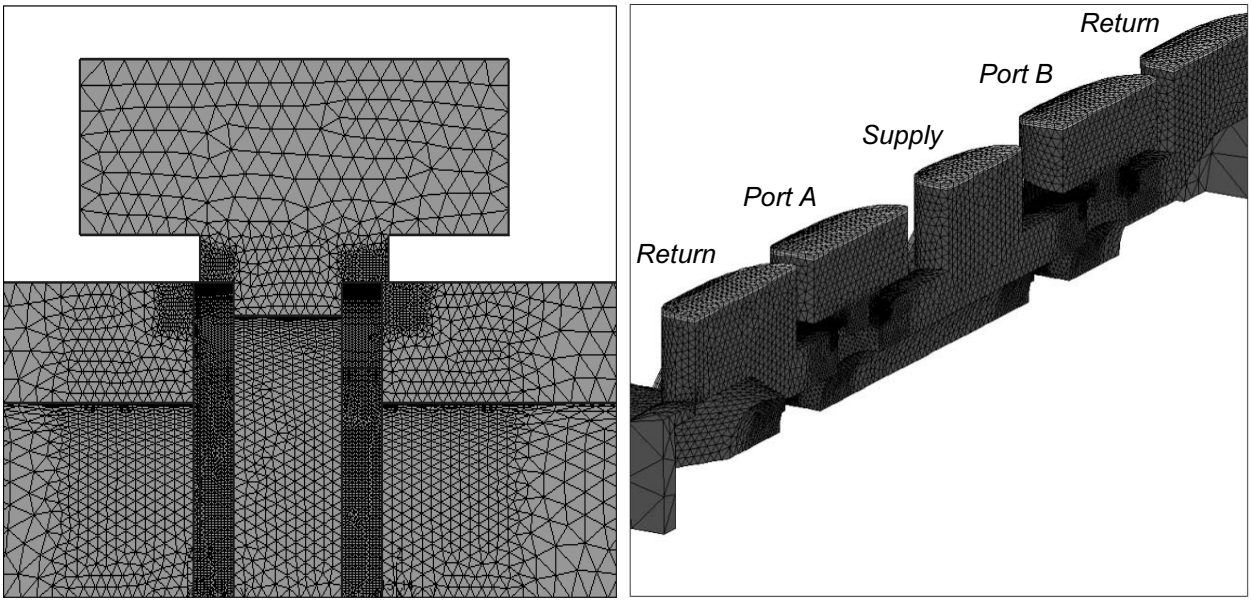

(a) (b)

Fig. 6: *Detail of the surface mesh (a) and volume mesh (b) on a CFD model*

3.2 Model Equations and Fluid Properties

The CFD simulation has been obtained by RANS equations combined with a Cubic/Low-Reynolds/k-ε turbulence model. This choice is basically justified by two reasons: firstly, the cubic stress-strain constitutive relation is more practicable than linear or quadratic formulas when the flow is characterised by strong curvature effects; secondly, the Low-Reynolds formulation is more accurate than the High-Reynolds one in describing complex internal flows, since the integration of the k-ε equations is made up to the walls, without introducing any empirical "wall function" (Bianchi and Fontanesi, 2003).

The fluid properties for the CFD analyses have been derived from the data of MIL-H-5606B, since it was the working fluid during the experiments (see section 2). Furthermore, the fluid has been assumed to be incompressible and cavitation phenomena have been neglected. All the simulations have been performed by initialising the turbulence length scale at 10% of the spool diameter, and the turbulence intensity to 0.05.

3.3 Test Cases for the CFD Analysis

The servovalve flow has been simulated with reference to sixteen positions of the spool, starting from the centred position up to the fully-opened valve, Table 1.a.

Concerning the boundary conditions, all the CFD models are characterised by a "pressure-type" condition (the "pressure-type" boundary condition on a surface is imposed by defining the mean value of the fluid pressure) on the supply and the return ports (set to 195 bar and 1 bar respectively), by a "wall-type" condition on the sleeve and the spool surfaces, and by a "symmetry-type" condition on the fluid surfaces created by the model reduction to one-quarter of the whole valve assembly.

The boundary conditions on port A and port B have been assumed as variable parameters of the analysis, by defining the four configurations reported in Table 1.b, where $\hat{P}_A$ ($\hat{P}_B$) is the surface mean value of the fluid pressure on port A (B), while $\mathbf{v}_A$ ($\mathbf{v}_B$) and $\mathbf{n}_A$ ($\mathbf{n}_B$) are the fluid velocity vector and the surface normal vector on port A (B) respectively. As a result, sixty-four CFD analyses have been performed. The number of test cases can appear rather large, but it has been necessary for the study of both turbulent and laminar flow conditions.

Table 1.a Test cases: spool positions

Model	1	2	3	4	5	6	7	8
x/x_{max} [%]	0	0.2	0.4	0.6	0.8	1	1.5	2
Model	9	10	11	12	13	14	15	16
x/x_{max} [%]	3.5	5	7.5	10	20	40	70	100

Table 1.b Test cases: boundary conditions on A-B ports

Parameter	$\hat{P}_A$	$\mathbf{v}_A \cdot \mathbf{n}_A$	$\hat{P}_B$	$\mathbf{v}_B \cdot \mathbf{n}_B$
a	N.D.	0	N.D.	0
b	98 bar	N.D.	98 bar	N.D.
c	125 bar	N.D.	70 bar	N.D.
d	160 bar	N.D.	35 bar	N.D.

N.D. = Not Defined

3.4 CFD Results

Some visualisations of the CFD results are reported in Fig. 7 and 10. All the plots refer to the boundary condition *c* (i.e. 70 bar pressure drop at the opening orifices, Table 1.b), but different spool displacements are considered.

Figure 7 shows a global three-dimensional map of the velocity vectors for test case *16-c* (i.e. fully-opened valve, Table 1). For the same test case, Fig. 8 reports two detailed section views of the servovalve flow, related to port A and port B respectively. In this simulation condition, the orifice flows are very energetic and the wall constraints induce minor effects on the discharge characteristics: actually, the values of both the orifice mean velocity (about 130 m/s) and the discharge angle (about 70°) are very near to those predicted by the classical orifice theory (Merritt, 1967). It should also be noted that the re-accelerating stream generated by the conic end of the spool (Fig. 8.b), which is responsible of a significant diminution of the flow force acting on the valve spool (Baudry and Mare, 2000). Wall constraints, three-dimensional effects and flow recirculation are shown to be more important if very small valve openings are considered. Figure 9 shows the orifice flows for the test case *8-c* (2% valve opening). The recirculation regions due to the walls induce a bending of the orifice veins, so that the discharge angles are near to 90°. In this flow condition, the energy dissipation is higher than in the case of fully-opened valve, since the recirculation regions are large and their energetic level is similar to that of the orifice flow. Figure 10 finally shows the velocity vectors in the orifice 3 for test case *13-c* (20% valve opening). In this condition, the orifice vein runs close to the spool piston as in the case *8-c* (Fig. 9.b), but the recirculation bubble in the annulus has been stretched and pulled away by the orifice flow, superseding the corner that leads to the return port. In this flow condition, the turbulence is less concentrated and the energy dissipation is lower, even than in the case of a fully-opened valve (note in Fig. 8.b that the orifice vein bends into the annulus, creating two recirculation regions).

The above-mentioned variation of the discharge characteristics has been pointed out by plotting the discharge coefficient for the orifice 3 (C_{d3}) as a function of the square root of the orifice Reynolds number (Re_3), Fig. 11. The calculation of C_{d3} and Re_3 has been obtained by Eq. 16 and 17,

$$C_{d3} = \frac{Q_{RB}}{A_3}\sqrt{\frac{\rho}{2(\hat{P}_B - \hat{P}_R)}} \tag{16}$$

$$Re_3 = \frac{2Q_{RB}}{\nu(w + x_v)} \tag{17}$$

where $\hat{P}_B$ and $\hat{P}_R$ are the surface mean values of the pressure on B and return ports, while Q_{RB} is the flow rate calculated on the B-side return port.

Figure 11 clearly shows that in the range of low Reynolds number ($0 < Re_3 < 300$) the discharge coefficient increases with the square root of the Reynolds number following a linear trend. This region includes the results related to all the spool displacements lower than the 2 % of the full valve stroke (all the test cases from 1 to 8, Table 1), as well as the results related to large valve openings that are characterized by a "wall-type" condition on A and B ports (e.g. the data given in Fig. 11 at $Re_3 \cong 20$ and $C_{d3} \cong 0.3$ is related to the test case *16-a*). This fact, confirmed by the experimental data reported in Fig. 4 where it can be noted that the "laminar range" has a similar extension, points out that the orifice flow must be considered laminar if very low pressure drop or (and) small valve openings are concerned.

On the other hand, the discharge coefficient predicted by CFD is essentially constant at high orifice Reynolds number ($Re_3 > 3000$). In this region, which includes the results related to the valve openings larger than the 70 % of the full-stroke and to orifice pressure drops higher than 35 bar, the orifice flow can be considered turbulent.

Concerning the laminar-to-turbulent transition, in accordance to the experimental results, it is characterized by a sort of "overshoot" in the C_d - Re curve, so that a significant diminution of the energy dissipation is predicted at intermediate Reynolds numbers (e. g. at $Re_3 \cong 800$, C_{d3} reaches its maximum, which is about

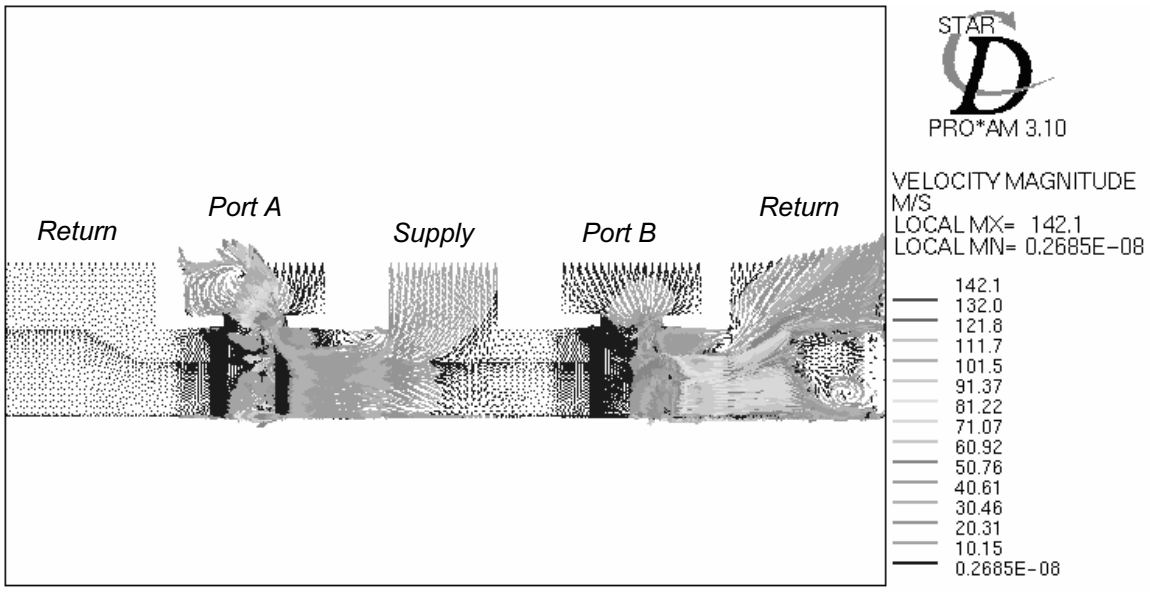

Fig. 7: *CFD results for test case 16-c (Table 1): velocity vectors*

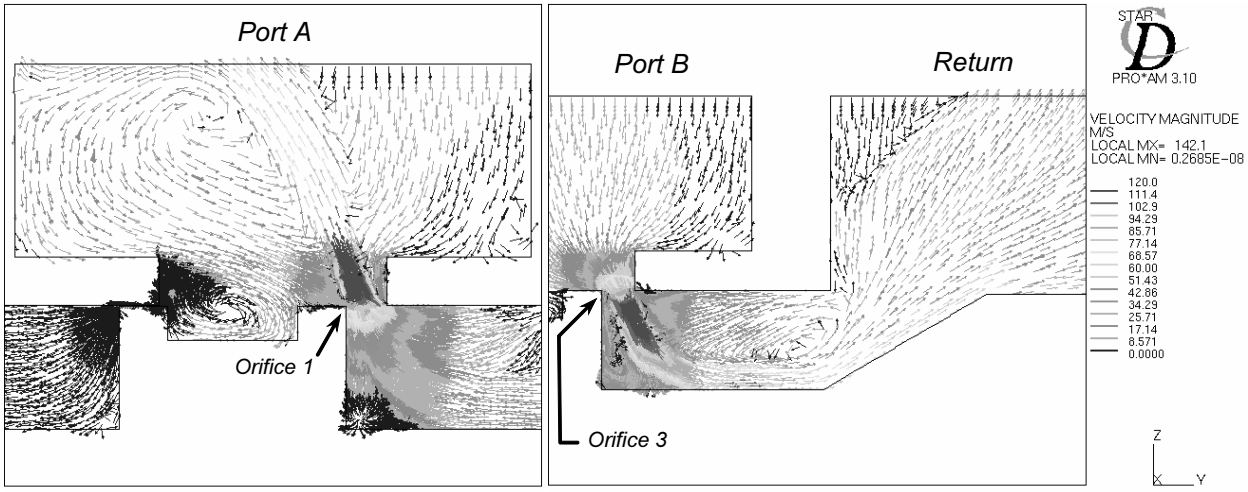

(a) Orifice flow on port A (b) Orifice flow on port B

Fig. 8: *CFD results for test case 16-c (Table 1): velocity vectors*

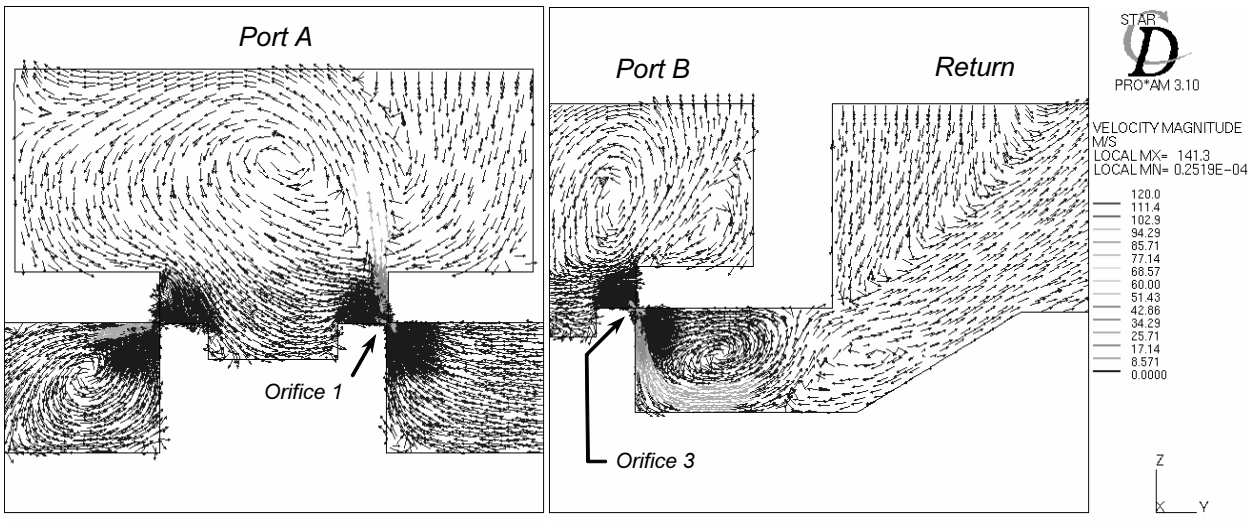

(a) Orifice flow on port A (b) Orifice flow on port B

Fig. 9: *FD results for test case 8-c (Table 1): velocity vectors*

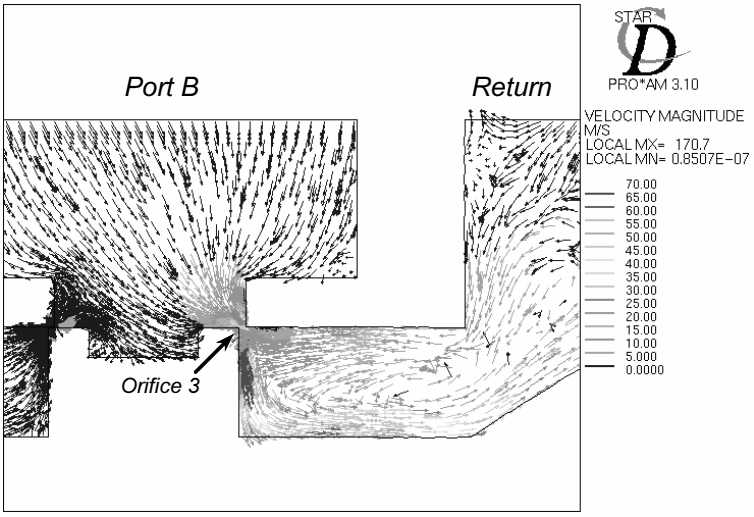

Fig. 10: *CFD results for test case 13-c (Table 1): velocity vectors*

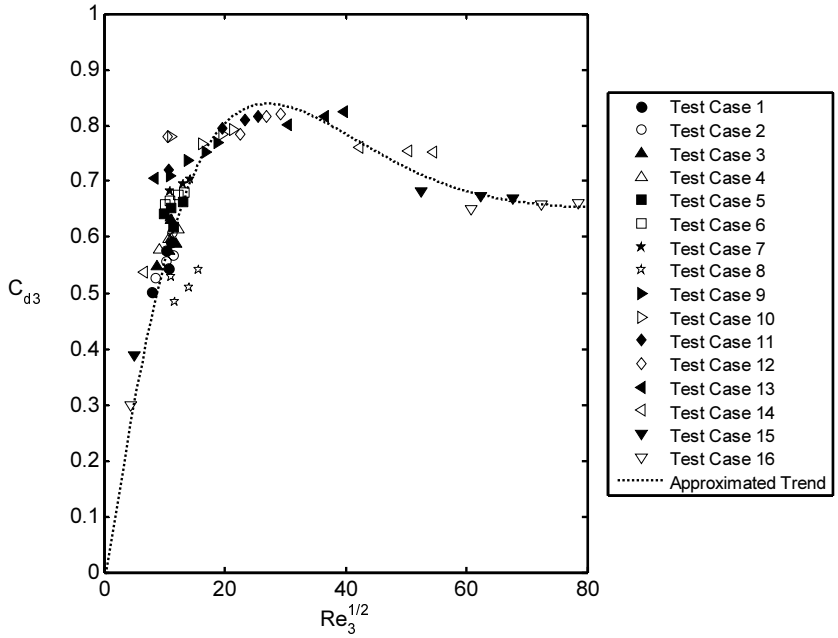

Fig. 11: *CFD results: discharge coefficient as a function of Reynolds number for orifice 3 (port B-return)*

0.85). This fact can be interpreted as an effect of the redistribution of the recirculation regions in the servovalve annulus. Actually, the data given in Fig. 11 at $Re_3 \cong 1400$ and $C_{d3} \cong 0.8$ is related to the test case 13-c, which is characterised, as earlier discussed, by the breakdown of a recirculation bubble in the servovalve annulus, Fig. 10.

Though the results of CFD simulations have been qualitatively verified by experiments, they provide erroneous predictions from a quantitative point of view. First of all, experimental data point out that the characteristics of the laminar-to-turbulent transition depend also on the valve opening, but this phenomenon is not observed in simulation. Secondly, experiments show that the servovalve flow is fully turbulent at $Re = 1000$, while CFD simulations predict that turbulence is well-established only for Reynolds numbers higher than 3000. In addition, the discharge coefficient for turbulent flow predicted by CFD is about 0.65, while the experimental value is about 0.58. Finally, the maximum experimental values of the discharge coefficient are located in the range of $Re \cong 300$ - 600 (depending on the valve opening), while CFD simulation locates the maximum discharge coefficient at $Re \cong 800$.

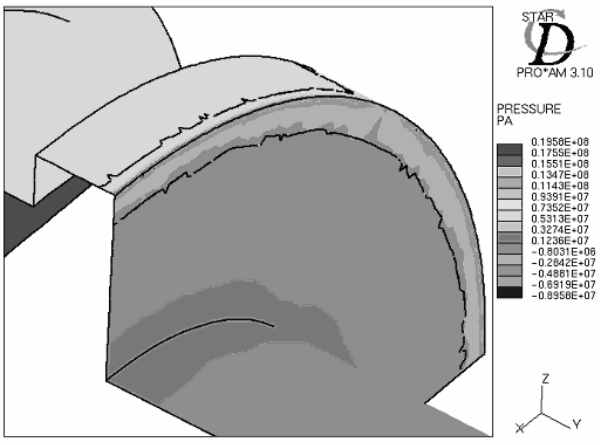

Fig. 12: *CFD results for test case 13-c (Table 1): pressures on the valve spool (edge of the orifice 3)*

These discrepancies must be essentially addressed to three causes. Firstly, the CFD simulation has been performed neglecting cavitation, whose effects can be relevant for a problem characterized by such strong pressure gradients (Koivula, 2000). In particular, CFD simulations highlighted the presence of regions with negative pressure values at the edges of the orifices, where cavitation is typically expected, Fig. 12.

As a second issue, the Reynolds numbers related to CFD analyses has been calculated by assuming a fixed fluid temperature (45° C), while during experiments the fluid temperature ranged from 35° C to 55° C. Finally, CFD models reproduce only one-quarter of the valve assembly, assuming a rotational-symmetric flow, which is rather stringent constraint especially because the servovalve flow is strongly three-dimensional.

Notwithstanding these aspects, CFD simulation provided important indications about the general characteristics of the servovalve flow, giving the possibility to interpret the experimental data starting from the knowledge of the discharge characteristics in the servovalve orifices.

Conclusions

Experiments and CFD simulations agree in predicting the characteristics of the laminar-to-turbulent flow transition in an aircraft-type four-way servovalve.

For both simulations and experiments, the orifice discharge coefficient is obtained as a function of the square root of the orifice Reynolds number, pointing out that a laminar behaviour is established when small orifice pressure drops or (and) very small valve openings are considered, while turbulence takes place for medium-high pressure drops and for medium-large valve openings, when the orifice Reynolds number is in the range of few thousands. At intermediate Reynolds numbers an increase of the discharge efficiency is observed on both experiments and CFD results. Flow visualisations are used to provide a physical interpretation to the phenomenon, achieving the conclusion that the energy dissipation lowers as a consequence of the breakdown of recirculation bubbles in the servovalve annulus.

Though the results of CFD simulations are qualitatively verified by experiments, they provide erroneous predictions from a quantitative point of view. These discrepancies have been essentially addressed to the hypotheses of the CFD model equations (cavitation neglecting, constant temperature) as well as to the assumptions about the flow characteristics (90°-rotational symmetric flow).

Acknowledgements

The author wants to thank Prof. Roberto Galatolo, for the coordination of the research activity, and Mr. Simone Gori, who contributed to the work during the period of his MSc Degree Thesis.

Nomenclature

n_A	Surface normal vector on port A	
n_B	Surface normal vector on port B	
v_A	Velocity vector on port A	[m/s]
v_B	Velocity vector on port B	[m/s]
w	Orifice area gradient	[m]
x_v	Valve spool displacement	[m]
x_{max}	Maximum valve opening	[m]
A_o	Orifice area	[m^2]
C_{do}	Orifice discharge coefficient	
C_{d1}	Orifice discharge coefficient for orifices 1 and 3	
D_L	Diameter of the load pipes	[m]
D_R	Diameter of the return pipe	[m]
D_S	Diameter of the supply pipe	[m]
L_L	Length of the load pipes	[m]
L_R	Length of the return pipe	[m]
L_S	Length of the supply pipe	[m]
K_o	Orifice leakage coefficient	[$m^3/s/Pa^{1/2}$]
K_1	Leakage coefficient for orifices 1 and 3	[$m^3/s/Pa^{1/2}$]
K_2	Leakage coefficient for orifices 2 and 4	[$m^3/s/Pa^{1/2}$]
P_A	Pressure on port A	[Pa]
$\hat{P}_A$	Surface mean value of the pressure on port A	[Pa]
P_B	Pressure on port B	[Pa]
$\hat{P}_B$	Surface mean value of the pressure on port B	[Pa]
P_R	Pressure on return port	[Pa]
$\hat{P}_R$	Surface mean value of the pressure on return port	[Pa]
P_S	Pressure on supply port	[Pa]
$P^{(m)}$	Measured value of pressure	[Pa]
Q_o	Orifice flow rate	[m^3/s]
Q_A	Flow rate on port A	[m^3/s]
Q_B	Flow rate on port B	[m^3/s]
Q_R	Flow rate on the return	[m^3/s]
Q_{RA}	Flow rate on the return (A-side)	[m^3/s]
Q_{RB}	Flow rate on the return (B-side)	[m^3/s]
Q_1	Flow rate through orifice 1	[m^3/s]
Q_2	Flow rate through orifice 2	[m^3/s]
Q_3	Flow rate through orifice 3	[m^3/s]
Q_4	Flow rate through orifice 4	[m^3/s]
Re_1	Reynolds number related to orifices 1 and 3	
Re_2	Reynolds number related to orifices 2 and 4	
Re	Reynolds number	
λ_L	Pressure loss coefficient related to the load pipes	
λ_R	Pressure loss coefficient related to the return pipe	
λ_S	Pressure loss coefficient related to the supply pipe	
ν	Fluid kinematic viscosity	[m^2/s]
ρ	Fluid density	[kg/m^3]
ΔP_o	Orifice pressure drop	[Pa]

References

Baudry, X. and **Mare, J. C.** 2000. Linking CFD and Lumped Parameters Analysis for the Design of Flow Compensated Spool Valves. *Proceedings of the 1st FPNI-PhD Symposium*, Hamburg (Germany), pp. 249-258.

Bianchi G. B. and **Fontanesi S.** 2003. On the Applications of Low-Reynolds Cubic k-ε Turbulence Models in 3D Simulations of ICE Intake Flows. *SAE Technical Paper Series* 2003-01-0003.

Borutzky W., **Barnard B.** and **Thoma J.** 2002. An Orifice Flow Model for Laminar and Turbulent Conditions. *Simulation Modelling Practice & Theory*, Vol. 10, N. 3, pp. 141-152.

Chen C. J. and **Jaw S. Y.** 1998. *Fundamentals of Turbulence Modelling*. Taylor & Francis.

Del Vescovo G. 2004. Experimental and Numerical Analysis of the Flow Forces on an Open-Centre Directional Control Valve. *Proceedings of the 3rd FPNI-PhD Symposium on Fluid Power*, Terrassa (Spain), pp. 83-92.

Gori S. 2005. *Development and Experimental Validation of CFD Models for the Characterisation of the Flow through Electro-Hydraulic Servovalves* (in Italian), Second Level Degree Thesis in Aerospace Engineering, University of Pisa.

Koivula T. 2000. On Cavitation in Fluid Power. *Proceedings of the 1st FPNI-PhD Symposium*, Hamburg (Germany), pp. 371-382.

Launder B. E. and **Spalding D. B.** 1972. *Mathematical Models of Turbulence.* Academic Press.

Merritt H. E. 1967. *Hydraulic Control Systems.* John Wiley & Sons.

Product data sheet: *Moog D633 and D634 Series Direct Drive Servo-Proportional Control Valves*, Moog Industrial Controls Division, Moog Inc. USA.

Software user guide: *STAR-CD Version 3.15 User Guide*. Computational Dynamics Limited, 2001.

Viall E. N. and **Zhang Q.** 2000. Determining the Discharge Coefficient of a Spool Valve. *Proceedings of the American Control Conference*, Chicago (USA), pp. 3600-3604.

Gianpietro Di Rito
The author (PhD Aerospace Engineering from 2005) currently works as a research consultant at the Department of Aerospace Engineering of the University of Pisa. His main areas of interest are: fluid power systems; design, modelling and simulation of flight control actuators; real-time/hardware-in-the-loop simulation of modern Flight Control Systems.